

Chaos-Driven Quantum State Discrimination Near Unit Fidelity

Sourav Paul ^{1,*}, Anant Vijay Varma ^{2,†}, Yogesh N. Joglekar ^{3,‡} and Sourin Das ^{1§}

¹ *Indian Institute of Science Education and Research Kolkata,
Mohanpur, Nadia 741246, West Bengal, India.*

² *Department of Physics, Ben-Gurion University of the Negev, Beer-Sheva 84105, Israel*

³ *Department of Physics, IU Indianapolis, LD 154,
402 N Blackford Street, Indianapolis IN 46202-3217, USA*

Distinguishing quantum states becomes exponentially difficult as their fidelity approaches unity, with diminishing success probabilities. This study revisits chaotic dynamics, leveraging their extreme sensitivity to initial conditions for rapid amplification of state discrimination measures. The discrete-time chaotic evolution of qubit states is generated via iterative application of a nonlinear conformal map on the Julia set. The "quantum microscope" is characterized by a magnification power quantified through a temporal Bell-type inequality. Fixed points of the conformal map are shown to dictate optimal measurement operators, enabling (a) well-defined magnification power and (b) bounded Bell-type inequality values, providing a device-independent framework for self-testing the microscope's performance.

Introduction:- Quantum metrology is one of the key ingredient in the efforts towards building efficient quantum computers [1–5]. Quantum-informatics techniques like quantum tomography [6–11], quantum state discrimination [12–18] have been proposed to identify an unknown quantum state. State manipulation protocols have also been put forward to evolve a pair of states effectively non-linearly [19–21] apart to discriminate them [22, 23]. These techniques accompany the restriction on the states which can be distinguished, ancillary macroscopic degrees of freedom and other *a priori* requirements.

In this letter we realize a "quantum microscope" [24], which allows distinction of a typical pair of states (PoS) of a qubit with arbitrary closeness. We apply fractional non-linear conformal (FNLC) maps iteratively to evolve a PoS on the Bloch sphere and exploit the fractal nature of the map [25, 26] to achieve high resolution. The novelty of our approach compared to the previous attempts is that it does not rely on orthogonality of the states to be distinguished rather exploits the random correlation between the measured *quantities*. We chose correlation coefficient [27] (r_{XY} in Eqn.[5]) between the observed values X and Y of measured quantities for each of the state in the PoS to characterize the microscope. We find that after finite iterations r_{XY} saturates to zero implying the "chaotic" nature of the dynamics independent of the closeness (δ) of a

typical PoS. It is worth mentioning that measuring fidelity (F) after iterative evolution of the PoS, is inefficient for states near unit fidelity initially. As the random nature of the dynamics restricts the average fidelity $\bar{F} = |\langle \Psi | \Phi \rangle|^2 = 1/2^N$ [40] (where $N = 1$ for a qubit and states $|\Psi\rangle$ and $|\Phi\rangle$ is the PoS considered.) Nevertheless, $\bar{F} = 1/2$ implies randomness (see SM [41] for plots).

We consider combination of two-time correlations (TTC) C_{ij} s similar to Bell-type correlations in order to calculate r_{XY} . For a dichotomic (*i.e.* eigenvalues ± 1 only) observable \hat{Q} the TTC C_{ij} , is defined as : $C_{ij} = \frac{1}{2} \langle \{\hat{Q}(t_i), \hat{Q}(t_j)\} \rangle$, where $\{\}$ is anti-commutator operation and $\hat{Q}(t_i)$ is the time evolved operator in the Heisenberg picture at two different times $t = 0 < t_i < t_j$. We find that calculating r_{XY} with even one TTC is enough to capture the "chaotic" nature of the dynamics and discriminate a PoS typically. Infact, for a suitable choice of measurement operator \hat{Q} , which is dictated by the roots of the FLNC map (see SM-[41]) $C_{ij} \approx \langle \hat{Q}(t_i) \rangle$. However, here we consider three-time measurement based Leggett-Garg (LG) parameter $K_3 = C_{12} + C_{23} - C_{13}$ [28–32] as the *quantity* to calculate r_{XY} . The reason is multi-fold: (a) LG parameter not only captures the required randomness to discriminate the states and reduces to $K_3 = C_{23} \approx \langle \hat{Q}(t_2) \rangle$ for appropriate choice of measurement operator \hat{Q} but also (b) violation of LG inequality *i.e.* $K_3 > 1$ guarantees a *faulty measurement device*. This allows self-testing of the microscope's performance in a device-independent manner. (c) Finally, for any given single PoS the difference between the K_3 parameters of each of the states allows to distinguish them in an experiment.

* souravpl2012@gmail.com; sp20rs034@iiserkol.ac.in

† anantvijay.cct@gmail.com

‡ yojoglek@iupui.edu

§ sourin@iiserkol.ac.in; sdas.du@gmail.com

FNLC maps and qubit dynamics:- Extended complex plane can be associated with the Bloch sphere via the stereographic projection, allowing for a projection $S : \mathcal{H} \rightarrow \tilde{C}$ from the two-dimensional projective Hilbert space \mathcal{H} to the extended complex plane \tilde{C} [33]. In the context of the Bloch sphere, a pure qubit state is represented as $|\psi\rangle = (\zeta_1, \zeta_2) = N(z, 1)^T$, where $N = 1/\sqrt{|z|^2 + 1}$ and the corresponding point on the extended complex plane is given by $z = \zeta_1/\zeta_2 = \cot \frac{\theta}{2} e^{i\phi}$ (ignoring the global phase) [33]. Any mathematical mapping $f(z)$ of the complex number z , can be projected back on the Bloch sphere. This projection can be thought of as a discrete time evolution, where the transformation $z \mapsto f(z)$ results in an “evolved state” [34]:

$$|\tilde{\psi}\rangle = \frac{1}{\sqrt{|f(z)|^2 + 1}} \begin{pmatrix} f(z) \\ 1 \end{pmatrix} \quad (1)$$

This expression capture how the qubit state evolves through the FNLC map over discrete time *i.e.* iteration. The following relation schematically shows the direct correspondence between the Bloch sphere state and a point on the extended complex plane: $|\psi\rangle \longleftrightarrow z \mapsto z' = f(z) \longleftrightarrow |\tilde{\psi}\rangle$. Since the map $f(z)$ can arbitrarily be defined, we consider FNLC maps of minimal order *i.e.* FNLC map of second order: $f(z) = p(z)/q(z)$, where $p(z) = az^2 + b; q(z) = cz^2 + d$. In particular we are interested in:

$$f(z) = \frac{z^2 + s}{sz^2 + 1} \quad (2)$$

This map under repeated iterations behaves in “regular” fashion in the Fatou set and in “chaotic” fashion in the Julia set. Parameter “ s ” controls the size of the Julia set of the map in Eq.(2) for the qubit dynamics. For $s = i$ the whole Bloch sphere corresponds to Julia set. The corresponding dynamics in the sense mentioned above has a stable fixed point determined by $f(z) = z \Rightarrow z = 1$ (see SM [41] for details). Just as the resolving power of a microscope depends on the wavelength of light, the minimum number of iterations needed to resolve any PoS depends upon the location of the PoS w.r.t. the stable fixed point [35].

Characterization of the Microscope:- We now present the statistical features of the microscope and issues related to optimization and measurement device induced errors. We begin the outline with the use of the statistical correlation r_{XY} between

the LG parameters (K_3 s) of ensemble of PoS for the characterization of the microscope. Thereafter we discuss various features of the microscope and discrimination of a given PoS.

LG parameter draws a boundary between the classical and the quantum correlations that a probability distribution retains as it evolves in time. In a minimal scenario, it requires at least three time instants to distinguish such correlations and this distinction is written in terms of in-equality: $K_3 = C_{12} + C_{23} - C_{13}, \leq 1$ [28–32], where C_{ij} s defined as $C_{ij} = \frac{1}{2} \langle \{\hat{Q}(t_i), \hat{Q}(t_j)\} \rangle$ are two-time correlations defined for a given choice of measurement operator $\hat{Q} = \hat{n} \cdot \vec{\sigma}$, where $\hat{n} = (\sin \theta_m \cos \phi_m, \sin \theta_m \sin \phi_m, \cos \theta_m)$ can be equivalently written as:

$$C_{ij} = \sum_{\hat{Q}(t_i/t_j)=\pm 1} \hat{Q}(t_i)\hat{Q}(t_j)P_{ij}(\hat{Q}(t_i), \hat{Q}(t_j)), \quad (3)$$

where P_{ij} s (see SM [41]) are the joint probabilities of observing outcome $\hat{Q}(t_i)$ and $\hat{Q}(t_j)$ at time instants t_i and t_j respectively. For this study, we discretize time and focus on the equispaced time interval with $t_1 = 0, t_2 - t_1 = n = t_3 - t_2$. We must emphasize that C_{ij} ’s are functions of n which in turn makes K_3 a function of n as well. It should also be noticed that for a given initial state $|\psi\rangle$ the time evolved state $e^{-iH(t_j-t_i)}|\psi\rangle$ has equivalent form $(f_{ij}^{(t_j-t_i)}(z_{|\psi\rangle}), 1)^T$ with $z_{|\psi\rangle}$ being the correspondent complex point to the state $|\psi\rangle$ after stereographic projection and where $f_{ij}^n(z) = f_{ij} \circ f_{ij} \circ \dots \circ f_{ij}(z)$ a composition of map f_{ij} (see SM [41] for details). We choose an ensemble of PoS as initial states, wherein the states of every pair has *separation* δ [36] in the complex plane. We then calculate r_{XY} after every iteration, which for two data set $X = \{x_1, x_2, \dots, x_L\}$ and $Y = \{y_1, y_2, \dots, y_L\}$ of population size L is given by:

$$r_{XY} = \frac{L \sum_i x_i y_i - (\sum_i x_i)(\sum_i y_i)}{\sqrt{[L \sum_i x_i^2 - (\sum_i x_i)^2][L \sum_i y_i^2 - (\sum_i y_i)^2]}} \quad (4)$$

Here, X and Y are LG parameters K_3 for two states from each pair of the ensemble. The outcome is demonstrated in the Fig 1, and the findings are: *i*) Correlation r_{XY} is able to capture the “chaotic” behavior of the discrete dynamics induced by FNLC map since in the large iteration limit r_{XY} stabilizes to 0. Although, it takes finitely many number of iterations depending upon δ before the states become

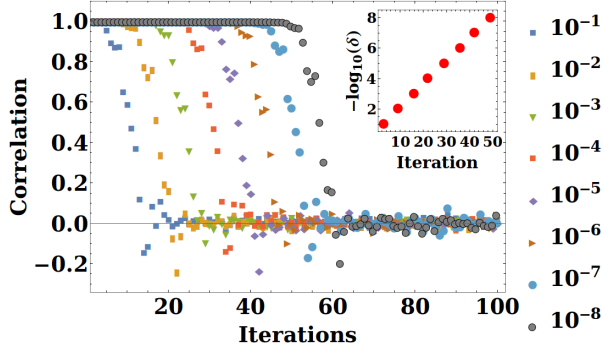


FIG. 1. **Statistical correlation (r_{XY}) vs iteration (n):** Here $\delta = 10^{-8}, 10^{-7}, \dots, 10^{-1}$ are different orders of separation in the initial PoS which are taken from the whole Bloch sphere for numerical calculation. The FNLC map corresponds to $s = i$ throughout the paper. For numerical calculations, ensemble of $10^4 (= 100 \times 100)$ in the complex plane) pair of points is chosen uniformly distributed on the whole Bloch sphere. We have chosen the dichotomic observable to be Pauli σ_x operator from here onwards unless mentioned. **Inset:** Critical number of iterations needed for discrimination vs the order of separation between the PoS.

distinguishable (not necessarily orthogonal). The randomness (*i.e.* $r_{XY} = 0$) in K_3 ensembles of PoS ensures that initial PoS is eventually separated on a measurable scale. *ii*) There is a hierarchy of cost for the magnification power (critical number of iterations) required, which grows linearly with the order of separation of initial PoS implying maximum exponential decay in the probability with n on an average [35].

Success probability of the dynamics:- The success probability of outcome after one iteration ($|\psi\rangle \rightarrow |\tilde{\psi}\rangle$) on one of the qubits for $s = i$ is

$$p_{\text{success}} = \frac{1 + |z|^4}{(1 + |z|^2)^2}, \quad (5)$$

where $\frac{1}{2} \leq p_{\text{success}} \leq 1$ as $0 \leq |z| \leq \infty$ (see SM[41]) shown in Fig.2. Also, the probability of success averaged over full Bloch sphere, after every iteration is $\langle p_{\text{success}} \rangle = 2/3$. Therefore, the average probability of the success of the dynamics after n^{th} iteration is roughly $(2/3)^n$. Nevertheless, the success probability of the dynamics after n iterations has lower bound of $(1/2)^n$, which is negligible for small separations and requires optimization.

Optimization of the success probability:- In Fig.2 and from Eq.(5) we note that the success rate of the dynamics is considerably large around the poles of Bloch sphere. We now chose patches around these poles to define the ensemble of initial PoS, shown as grey shaded region (only for north pole belt shown) in the Fig.2. Calculation of r_{XY} for this patch with the separation between PoS being 10^{-8} is illustrated in the Fig.2 (Inset) (for south pole patch the inset figure yields same qualitative graph). We note that though r_{XY} is a statistical *quantity*, it works as a good measure of discrimination for small patches as well, as long as the ensemble size is enough. The least value of probability in the shaded regions is ≈ 0.95 and about $n = 60$ iterations (considering worst case) are enough for the correlations to saturate to zero. This implies that even the microscopic distance of the order of $\delta = 10^{-8}$ is distinguishable by this protocol successfully with the probability $> \approx 0.05$. Therefore, *a priori* information of the whereabouts of the PoS can drastically improve the success probability of the dynamics.

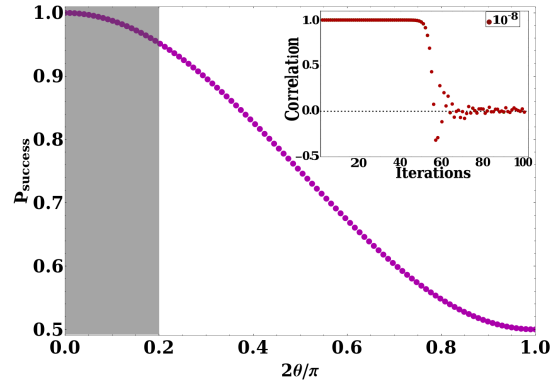


FIG. 2. **Optimization of the state discrimination protocol:** Success probability in Eq.5 wrt θ (colatitude). **Inset:** r_{XY} vs n for the initial PoS (chosen from the north pole region belt (red) with $\theta = 0$ to $\theta = \pi/10$, which are $\delta = 10^{-8}$ distance apart. For numerical calculations, same ensemble size and the measurement operator have been used as in Fig. 1.

Faulty Measurement Device:- We now argue how a *faulty measuring device* can be detected if we use LG parameter based correlation instead of measuring the expectation value of \hat{Q} in time. Recall that $C_{ij} = P_{ij}(\uparrow, \uparrow) - P_{ij}(\uparrow, \downarrow) - P_{ij}(\downarrow, \uparrow) + P_{ij}(\downarrow, \downarrow)$. Also, consider the root $z = 1$ for the eqn. $f(z) = z$, which corresponds to $\hat{n} = \hat{i}$ direction. we can now define the measurement operator to be $\hat{Q} = \vec{\sigma} \cdot \hat{n} = \sigma_x$. Let us now assign the probabilities of measuring

\uparrow and \downarrow at time instant t_i to be α and β respectively ($\alpha + \beta = 1$). However, once we have measured the states at time instant t_i resulting in one of the eigenstates of the σ_x we know *a priori* the probabilities at time instant t_j as the eigenstates of the σ_x are fixed points of the dynamics. This allows us to write $C_{ij} = \alpha - \beta = \langle \psi_{t_i} | \hat{Q} | \psi_{t_i} \rangle = \langle \hat{Q}(t_i) \rangle$. Since in this protocol we have considered $t_1 = 0; t_2 = n$ and $t_3 = 2n$ and the dynamics cease once measured implies $C_{12} = C_{13}$. Therefore, $-1 \leq K_3 = C_{23} = \langle \hat{Q}(t_2) \rangle = \langle \hat{Q}(n) \rangle \leq 1$ *i.e.* LG inequality is satisfied, if the measuring device is ideal. However, once we have *faulty measurement device i.e.* error in (θ_m, ϕ_m) , LGI is violated *independent* of the choice of PoS. This fact is illustrated in Fig.3 for a randomly selected state on the Bloch sphere. Since the FLNC map discussed here is not a CPTP map, and is the example of non-Hermitian dynamics we expect the LG parameter to even violate Luder's bound [37, 38].

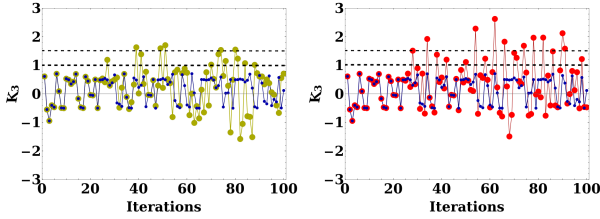


FIG. 3. **Sensitivity to the faulty measuring device:** Variation of LG Parameter K_3 wrt iteration for randomly chosen initial states. In both the plots blue markers represent evolution interrupted with an ideal measurement device. While, green marker in (a) shows K_3 time series with an error of order 10^{-8} in azimuthal angle ϕ_m & (b) same order of error in longitudinal angle θ_m (red) of the measurement operator.

Discriminating a given PoS:- After discussing the characterization and issues related to errors, we finally illustrate how to distinguish any given PoS. While Fig. 1 displays a *typical* scenario, it is essential to show how to distinguish a given PoS in an experiment. For this purpose we calculate LG parameters for each of the states in the PoS after every iteration and the first non-zero value in their difference marks the number of iterations needed to distinguish the states. Note that $K_3 = \langle \hat{Q}(t_2) \rangle = \langle \sigma_x(n) \rangle$. Representative cases for different orders of separation δ are displayed in the Fig. 4. As mentioned above the resolution power of the microscope depends upon the location of the PoS wrt fixed point of the dynamics. We demonstrate this statement in the Fig. 5 for PoS selected on the Bloch sphere (southern hemisphere).

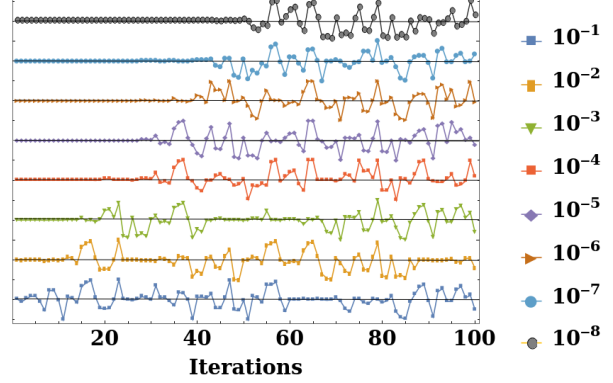


FIG. 4. **Difference of K_3 vs iteration:** for an initial PoS chosen randomly from the Bloch sphere. Fluctuation in each curve represents non-zero value of the difference of K_3 for the chosen PoS. Different colors are the initial separation δ (of the form 10^{-n}) between the states. Each curve is bounded from -2 to 2 (y-axis) with the flat lines marking zero value for all cases.

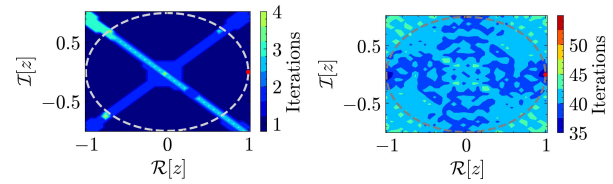


FIG. 5. **Resolution heat map:** Discrimination of different PoS in the complex plane, using the difference of K_3 values. Each point in the plane represents a PoS with separation (a) $\delta = 10^{-1}$ and (b) $\delta = 10^{-8}$. Color is the minimum number of iterations required for non-zero difference of K_3 values. In both the plots dashed circle marks the boundary of southern hemisphere and red dot indicates the stable fixed point of the dynamics.

Circuit implementation of the dynamics:- We finally discuss the implementation of the discrete dynamics induced by FNLC maps using quantum gates. We begin with an ensemble of “quantum circuit units” (QCU) in Fig.6. Identical initial states $|\Psi\rangle = |\psi\rangle \otimes |\psi\rangle$ are fed into QCU, which first implement a unitary gate $U_{\text{comp}} = U_{\text{gate}} U_{\text{XOR}}$ on the two qubit state $|\Psi\rangle$. After that one of the qubits is projected onto the $|\uparrow\rangle_z$ states via projection $\hat{P} = \mathbf{I} \otimes |\uparrow\rangle_z \langle \uparrow|$. This leads to transformation of the remaining qubit to $|\tilde{\psi}\rangle$ in Eq.(1). This completes the gate implementation required for each iteration (details in SM [41]).

Summary:- To summarize, we have investigated a possibility of a high resolution “*quantum micro-*

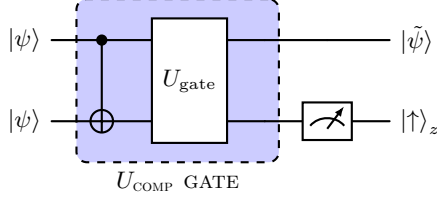


FIG. 6. **Quantum circuit unit (QCU) of FLNC map:** of the form $f(z) = \frac{z^2 + s}{sz^2 + 1}$. In the left of the quantum circuit, a separable state $|\psi\rangle \otimes |\psi\rangle$ is fed as input which generates an output state $|\tilde{\psi}\rangle \otimes |\uparrow\rangle_z$ after post-selection of which the renormalized state of the 1st qubit mimics the evolution generated by FNLC map (Eq.2).

scope” for a qubit exploiting the fractal nature of discrete emulated dynamics. The highlights of this study are (i) the statistical correlation r_{XY} can efficiently characterize this microscope for optimized

choice of the measurement operator. This correlation captures the “chaotic” nature of the discrete dynamics and can be utilized as an alternative to the Lyapunov Exponents. In general, the cost of distinguishing the states increases exponentially with the decrease in the initial distance between them and therefore, exponentially larger QUCs are required for higher resolution in this protocol [35]. (ii) The difference of LG parameters of the two states in PoS is enough to discriminate them in an experiment. (iii) The LG inequality acts as a testbed for detecting a faulty measurement device.

Acknowledgment:- S.P. offers his gratitude to the Council of Scientific and Industrial Research (CSIR), Govt. of India for financial support. A.V.V. would like to acknowledge the Israel Science Foundation (Grant No.518/22) for funding. S.P. and A.V.V. contributed equally to this work.

-
- [1] Vittorio Giovannetti, Seth Lloyd, and Lorenzo Maccone, “Advances in quantum metrology,” *Nature Photonics* **5**, 222–229 (2011).
 - [2] Vittorio Giovannetti, Seth Lloyd, and Lorenzo Maccone, “Quantum metrology,” *Phys. Rev. Lett.* **96**, 010401 (2006).
 - [3] “Front matter,” in *Quantum Metrology: Foundation of Units and Measurements* (John Wiley & Sons, Ltd, 2015) pp. I–XVI.
 - [4] Géza Tóth and Iagoba Apellaniz, “Quantum metrology from a quantum information science perspective,” *Journal of Physics A: Mathematical and Theoretical* **47**, 424006 (2014).
 - [5] Luca Pezzè, Augusto Smerzi, Markus K. Oberthaler, Roman Schmied, and Philipp Treutlein, “Quantum metrology with nonclassical states of atomic ensembles,” *Rev. Mod. Phys.* **90**, 035005 (2018).
 - [6] Alessandro Bisio, Giulio Chiribella, Giacomo Mauro D’Ariano, Stefano Facchini, and Paolo Perinotti, “Optimal quantum tomography,” *IEEE Journal of Selected Topics in Quantum Electronics* **15**, 1646–1660 (2009).
 - [7] Ryan O’Donnell and John Wright, “Efficient quantum tomography,” in *Proceedings of the Forty-Eighth Annual ACM Symposium on Theory of Computing*, STOC ’16 (Association for Computing Machinery, New York, NY, USA, 2016) p. 899–912.
 - [8] R. T. Thew, K. Nemoto, A. G. White, and W. J. Munro, “Qudit quantum-state tomography,” *Phys. Rev. A* **66**, 012303 (2002).
 - [9] Matthias Christandl and Renato Renner, “Reliable quantum state tomography,” *Phys. Rev. Lett.* **109**, 120403 (2012).
 - [10] G. M. D’Ariano and P. Lo Presti, “Quantum tomography for measuring experimentally the matrix elements of an arbitrary quantum operation,” *Phys. Rev. Lett.* **86**, 4195–4198 (2001).
 - [11] A. I. Lvovsky and M. G. Raymer, “Continuous-variable optical quantum-state tomography,” *Rev. Mod. Phys.* **81**, 299–332 (2009).
 - [12] János A. Bergou, “Discrimination of quantum states,” *Journal of Modern Optics* **57**, 160–180 (2010).
 - [13] Carl W. Helstrom, “Quantum detection and estimation theory,” (1976).
 - [14] I.D. Ivanovic, “How to differentiate between non-orthogonal states,” *Physics Letters A* **123**, 257–259 (1987).
 - [15] Stephen M. Barnett and Sarah Croke, “Quantum state discrimination,” *Adv. Opt. Photon.* **1**, 238–278 (2009).
 - [16] Ashley Montanaro, “On the distinguishability of random quantum states,” *Communications in Mathematical Physics* **273**, 619–636 (2007).
 - [17] Marcus Cramer, Martin B. Plenio, Steven T. Flammia, Rolando Somma, David Gross, Stephen D. Bartlett, Olivier Landon-Cardinal, David Poulin, and Yi-Kai Liu, “Efficient quantum state tomography,” *Nature Communications* **1**, 149 (2010).
 - [18] Carl M. Bender, Dorje C. Brody, João Caldeira, Uwe Günther, Bernhard K. Meister, and Boris F. Samsonov, “Pt-symmetric quantum state discrimination,” *Philosophical Transactions of the Royal*

- Society A: Mathematical, Physical and Engineering Sciences **371**, 20120160 (2013).
- [19] H. Bechmann-Pasquinucci, B. Huttner, and N. Gisin, “Non-linear quantum state transformation of spin-12,” *Physics Letters A* **242**, 198–204 (1998).
- [20] Salman Habib, Kurt Jacobs, and Kosuke Shizume, “Emergence of chaos in quantum systems far from the classical limit,” *Phys. Rev. Lett.* **96**, 010403 (2006).
- [21] M J Everitt, “On the correspondence principle: implications from a study of the nonlinear dynamics of a macroscopic quantum device,” *New Journal of Physics* **11**, 013014 (2009).
- [22] Vaibhav Madhok, Carlos A. Riofrío, Shohini Ghose, and Ivan H. Deutsch, “Information gain in tomography—a quantum signature of chaos,” *Phys. Rev. Lett.* **112**, 014102 (2014).
- [23] Juan Mauricio Torres, József Zsolt Bernád, Gernot Alber, Orsolya Kálmán, and Tamás Kiss, “Measurement-induced chaos and quantum state discrimination in an iterated tavis-cummings scheme,” *Phys. Rev. A* **95**, 023828 (2017).
- [24] Seth Lloyd and Jean-Jacques E. Slotine, “Quantum feedback with weak measurements,” *Phys. Rev. A* **62**, 012307 (2000).
- [25] Dietmar Saupe, “Efficient computation of julia sets and their fractal dimension,” *Physica D: Nonlinear Phenomena* **28**, 358–370 (1987).
- [26] Septima Poinsette Clark, “Estimating the fractal dimension of chaotic time series,” *Lincoln Laboratory Journal* **3** (1990).
- [27] David Freedman, Robert Pisani, and Roger Purves, “Statistics (international student edition),” Pisani, R. Purves, 4th edn. WW Norton & Company, New York (2007).
- [28] A. J. Leggett and Anupam Garg, “Quantum mechanics versus macroscopic realism: Is the flux there when nobody looks?” *Phys. Rev. Lett.* **54**, 857–860 (1985).
- [29] Clive Emary, Neill Lambert, and Franco Nori, “Leggett–garg inequalities,” *Reports on Progress in Physics* **77**, 016001 (2013).
- [30] M. E. Goggin, M. P. Almeida, M. Barbieri, B. P. Lanyon, J. L. O’Brien, A. G. White, and G. J. Pryde, “Violation of the leggett–garg inequality with weak measurements of photons,” *Proceedings of the National Academy of Sciences* **108**, 1256–1261 (2011).
- [31] George C. Knee, Stephanie Simmons, Erik M. Gauger, John J.L. Morton, Helge Riemann, Nikolai V. Abrosimov, Peter Becker, Hans-Joachim Pohl, Kohei M. Itoh, Mike L.W. Thewalt, G. Andrew D. Briggs, and Simon C. Benjamin, “Violation of a leggett–garg inequality with ideal non-invasive measurements,” *Nature Communications* **3**, 606 (2012).
- [32] Vikram Athalye, Soumya Singha Roy, and T. S. Mahesh, “Investigation of the leggett-garg inequality for precessing nuclear spins,” *Phys. Rev. Lett.* **107**, 130402 (2011).
- [33] Jae-weon Lee, Chang Ho Kim, Eok Kyun Lee, Jaewan Kim, and Soonchil Lee, “Qubit geometry and conformal mapping,” *Quantum Information Processing* **1**, 129–134 (2002).
- [34] Sourav Paul, Anant Vijay Varma, and Sourin Das, “Fractional conformal map, qubit dynamics and the leggett–garg inequality,” *Journal of Physics A: Mathematical and Theoretical* **57**, 385203 (2024).
- [35] András Gilyén, Tamás Kiss, and Igor Jex, “Exponential sensitivity and its cost in quantum physics,” *Scientific Reports* **6**, 20076 (2016).
- [36] If the two states of the PoS in the complex plane are z_1 and z_2 , then $\delta = |z_1 - z_2|$. Moreover, stereographic projection of the states on the Bloch sphere only overestimates the critical number of iterations needed for distinguishability. Therefore, we only consider half of the Bloch sphere in Fig 5.
- [37] Anant V Varma, Ipsika Mohanty, and Sourin Das, “Temporal correlation beyond quantum bounds in non-hermitian pt- symmetric dynamics of a two level system,” *Journal of Physics A: Mathematical and Theoretical* **54**, 115301 (2021).
- [38] Anant V. Varma, Jacob E. Muldoon, Sourav Paul, Yogesh N. Joglekar, and Sourin Das, “Extreme violation of the leggett-garg inequality in nonunitary dynamics with complex energies,” *Phys. Rev. A* **108**, 032202 (2023).
- [39] For the FNLC map with $s = i$ (Eq. 2), taking $\theta_0 = \theta$, $\phi_0 = \phi$ one can write
- $$\theta_n = 2 \cot^{-1} \left[\sqrt{\frac{3 + \cos 2\theta_{n-1} + 2 \sin^2 \theta_{n-1} \sin 2\phi_{n-1}}{3 + \cos 2\theta_{n-1} - 2 \sin^2 \theta_{n-1} \sin 2\phi_{n-1}}} \right]$$
- and
- $$\phi_n = -2 \tan^{-1} \left[\frac{\cos \theta_{n-1}}{\cos 2\phi_{n-1} \sin^2 \theta_{n-1}} \right]$$
- where $z_n = f^{(n)}(z) = \cot\left[\frac{\theta_n}{2}\right]e^{i\phi_n}$ with z_n being the complex number corresponding to n -th iterated state.
- [40] J. Chalker, <http://www-thphys.physics.ox.ac.uk/talks/CMTjournalclub/sources/orthogc.pdf> (2015).
- [41] In the supplementary we provide details of the FNLC maps and its Julia set, success probability of the emulated discrete dynamics, calculation of discrete time LGI and details of quantum circuit implementation for n th iteration.

Chaos-Driven Quantum State Discrimination Near Unit Fidelity

Sourav Paul, Anant Vijay Varma, Yogesh N. Joglekar, and Sourin Das

(Supplementary Material)

In this supplementary we provide details of the FLNC maps and its Julia set, success probability of the emulated discrete dynamics, calculation of discrete time LGI, details of quantum circuit implementation for n th iteration.

==== [1] Fractal nature of the FNLC map $f(z)$

FNLC maps show fractal nature upon repeated iteration. Below we show Julia set of this FNLC map (given in main text Eq.(2)) for different s parameter value (in Fig.7). Behaviour of Julia set can be measured using various fractal dimensions [26]. In the Fig.8 we show the Box dimension as a function of control parameter s .

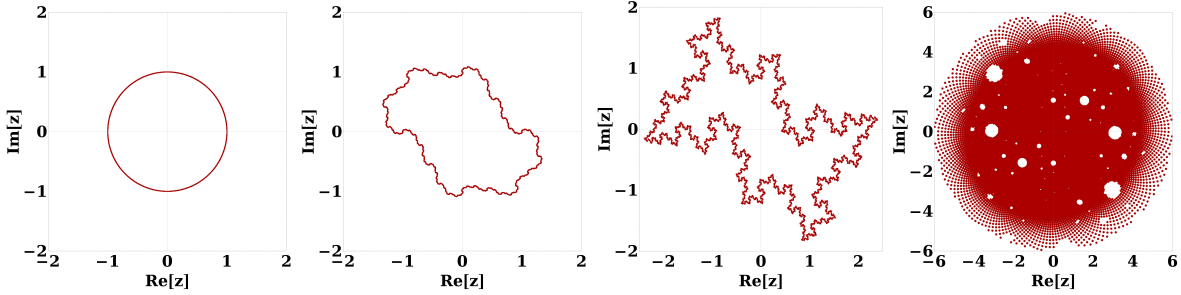


FIG. 7. Julia Set plots in complex z plane with increasing value of parameter s . Corresponding s values are 0, $0.25i$, $0.5i$, $0.99i$ from left to right respectively.

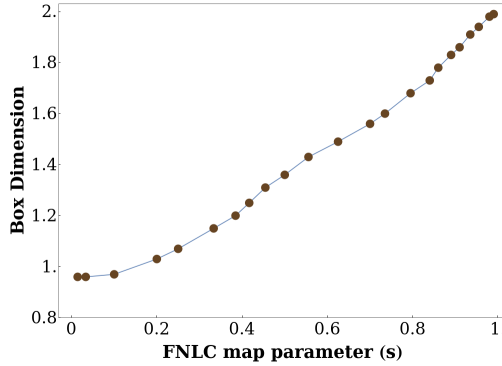


FIG. 8. Plot of Box dimension (fractal dimension) as function of s parameter of the FNLC map (Eq.2).

==== [2] Discrete Time LGI with FNLC Maps and Evaluation of Statistical Correlation r_{XY}

In this supplementary section, we outline the procedure for evaluating the three-time Leggett-Garg (LG) parameter K_3 (given in maintext) within the framework of discrete-time evolution governed by FNLC maps.

These maps are described by Eq.(2), with the measurement process characterized by the dichotomic operator $\hat{Q} = \vec{\sigma} \cdot \hat{n}$. The evaluation involves the following systematic steps:

Steps: (i) Initial Evolution ($t_1 \rightarrow t_2$): The state of the qubit system at the initial time t_1 is represented by the complex coordinate $z = z_1$ on the extended complex plane. The evolution from t_1 to t_2 is induced by the map $f_{12}(z)$ (the same map used in Eq.(2)), which acts on the initial state.

(ii) Subsequent Evolution ($t_2 \rightarrow t_3$): The system then evolves over the next time interval t_2 to t_3 . The state at time t_2 , denoted by $z = z_2 = f_{12}(z_1)$, undergoes further evolution governed by the map $f_{23}(z)$ (the same map used in Eq.(2)).

(iii) Composite Evolution ($t_1 \rightarrow t_3$): The total evolution from the initial time t_1 to the final time t_3 is described by the composition of the individual maps. Explicitly, the composite map $f_{13} = f_{23} \circ f_{12}$ acts on the initial state z_1 , thereby encapsulating the overall system dynamics across the three discrete time steps.

$$z_2 = f_{12}(z_1) = \frac{z_1^2 + s}{s z_1^2 + 1}; \quad z_3 = f_{23}(z_2) = \frac{z_2^2 + s}{s z_2^2 + 1}$$

$$z_3 = f_{23}(f_{12}(z_1)) = \frac{\left(\frac{z_1^2 + s}{s z_1^2 + 1}\right)^2 + s}{s \left(\frac{z_1^2 + s}{s z_1^2 + 1}\right)^2 + 1} \quad (6)$$

Joint Probabilities (P_{ij}): The temporal correlations C_{ij} 's (given in main text) are expressed in terms of joint probabilities P_{ij} 's which are required to evaluate the LG parameter K_3 for the dichotomic observable $\hat{Q} = \vec{\sigma} \cdot \hat{n}$.

$$P_{ij}(\hat{Q}(t_i), \hat{Q}(t_j)) = \frac{(|\langle \pm_Q | e^{-iH(t_j - t_i)} | \pm_Q \rangle|^2) (|\langle \pm_Q | e^{-iH(t_i - t_1)} | \psi^{(0)} \rangle|^2)}{\langle \pm_Q | e^{iH^\dagger(t_j - t_i)} e^{-iH(t_j - t_i)} | \pm_Q \rangle \langle \pm_Q | e^{iH^\dagger(t_i - t_1)} e^{-iH(t_i - t_1)} | \psi^{(0)} \rangle} \quad (7)$$

where, $i < j$ $\{i, j = 1, 2, 3\}$ and $|\psi^{(0)}\rangle$ is describing initial state. Here $\hat{Q}(t_k)$ denotes the measurement outcome either +1 (corresponding to the $|\uparrow\rangle_n$) or -1 (corresponding to the $|\downarrow\rangle_n$) of dichotomic observable $\hat{Q} = \vec{\sigma} \cdot \hat{n}$. It is to be pointed out that, the state $e^{-iH(t_j - t_i)}|\phi\rangle$ is equivalent to the state $(f_{ij}(z_{|\phi\rangle}), 1)^T$ where $z_{|\phi\rangle}$ is complex point residing in complex plane referring the state $|\phi\rangle$ on the Bloch sphere via stereographic projection. Also $f_{ii}(z_{|\phi\rangle}) = z_{|\phi\rangle}$ for all $\{i = 1, 2, 3\}$. The $f_{ij}(z_{|\psi\rangle})$ is the same map as described by Eq.(6).

Using the expression of FNLC map (Eq.(6)), we find out the joint probabilities (Eq.(7)) and thereafter the correlation functions (C_{ij}) (given in main text Eq.(3)), corresponding to a initial state lying on the Bloch sphere undergoing discrete time evolution induced by FNLC maps (of the form Eq.(2)) for the dichotomic measurement operator $\hat{Q} = \vec{\sigma} \cdot \hat{n}$ (Eq.(6)-Eq.(7)).

Generation of K_3 data series over iteration for ensemble of states: The above process summarizes the generation of K_3 data series over iteration (discrete time) for a specific initial state with a fixed dichotomic observable and a specific FNLC map. This process can be replicated for an ensemble of different initial states carefully chosen from the Julia set of a specific FNLC map (Eq.2) lying on the Bloch sphere.

Evaluation of r_{XY} : To evaluate statistical correlation (r_{XY}) (in main text Eq.(4)) for the ensemble of K_3 data series, we first generate the K_3 data series for initial and corresponding paired states from the different PoS which are δ distance apart on the Bloch sphere taken from the Julia set. Next fixing an particular iteration(n) value, we collect all the K_3 data i) for every initial state for that n and call that data set as X , ii) for the corresponding pair of the initial states for that n and call that data set Y . After that we find the standard statistical correlation (r_{XY}) for these two data sets and plot them as a function of n (no. of iteration).

===== [3] Average Fidelity for pairs of initial states

In this supplementary section we evaluate average fidelity between PoS, which are separated by δ distance initially, lying on the Julia set of the Bloch sphere of the FNLC maps. We define the fidelity as,

$$F(n) = |\langle \psi_\delta(n) | \psi(n) \rangle|^2 \quad \text{with} \quad |\psi(n)\rangle = \frac{1}{\sqrt{1 + |f^{(n)}(z)|^2}} \begin{pmatrix} f^{(n)}(z) \\ 1 \end{pmatrix}, \quad |\psi_\delta(n)\rangle = \frac{1}{\sqrt{1 + |f^{(n)}(z_\delta)|^2}} \begin{pmatrix} f^{(n)}(z_\delta) \\ 1 \end{pmatrix} \quad (8)$$

where $|\psi(n)\rangle$ and $|\psi_\delta(n)\rangle$ corresponds to state and pair partner of that state separated by distance δ , with z and z_δ being the complex points corresponding to initial state and its pair of the PoS for $n = 0$. n denotes the iteration.

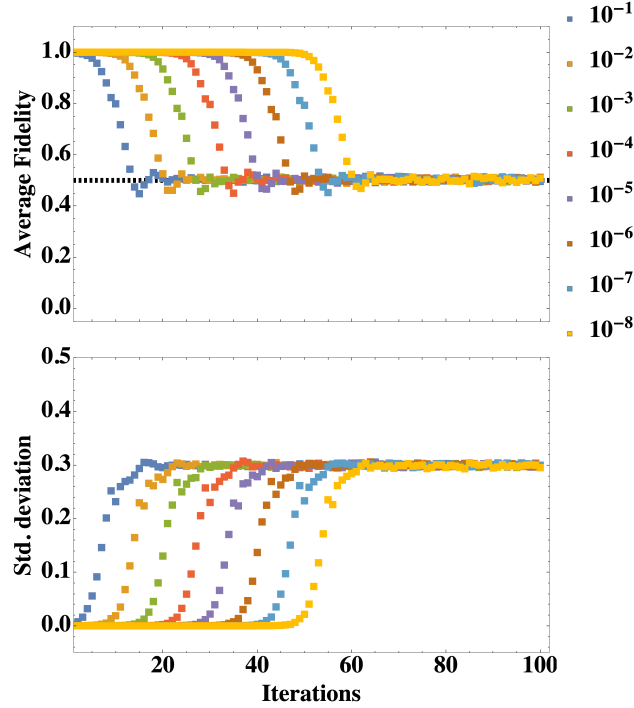


FIG. 9. **Average & std. deviation of Fidelity vs iterations (n):** Here $\delta = 10^{-1}, \dots, 10^{-8}$ suggests the separation of the initial PoS which are taken from the whole Bloch sphere for numerical calculation. Here the $s = i$. Here we take 10^4 ($=100 \times 100$) points uniformly distributed over the Julia set of the whole Bloch sphere.

Following the same procedure for choosing initial states as discussed in main text, we evolve both the initial states and the correspondent paired states via the FNLC map (Eq.(2)) which are chosen from the Julia set of the Bloch sphere and evaluate the fidelity as a function of n (iteration). Next we take the average of the fidelity found for each pair of initial states separated by δ distance and plot them as function of n along with standard deviation. The outcome is demonstrated in the Fig 9, and the findings are: *i*) Average fidelity fails to distinguish a typical PoS, as fidelity saturates to highly non-zero value along with fact that standard deviation around the average fidelity is typically large for all scales of separation of the initial PoS. *ii*) It is although interesting to note that average fidelity guides in detecting the critical iteration to look for to perform the statistical correlation measure.

[4] Quantum Circuit for generating n -th iteration of FNLC map

In this supplementary section we elaborately discuss the implementation of the FNLC map $f(z) = \frac{z^2+s}{sz^2+1}$ (where s being purely imaginary varying from $s = 0$ to $s = i$) starting from identical two qubit system. We evolve the two qubit system via 4×4 unitary matrix only to measure the 2nd qubit in the σ_z 's positive eigenstate at the end. This measurement induced state via post-selection generates a non unitary evolution of the first qubit with some finite success rate which one can post-select and renormalize to make it a pure state on the Bloch sphere. Below we give a brief mathematical description of the same. One starts with the initial two qubit seperable state as,

$$\begin{aligned} |\Psi\rangle &= |\psi\rangle \otimes |\psi\rangle = \frac{1}{\sqrt{1+|z|^2}} \begin{pmatrix} z \\ 1 \end{pmatrix} \otimes \frac{1}{\sqrt{1+|z|^2}} \begin{pmatrix} z \\ 1 \end{pmatrix} \\ &= \frac{1}{1+|z|^2} \begin{pmatrix} z^2 \\ z \\ z \\ 1 \end{pmatrix} \end{aligned} \quad (9)$$

Next one implements two 2-qubit unitary gates U_{XOR} and U_{gate} (FIG.6) in succession. The matrix form of the gates are

$$U_{XOR} = \begin{pmatrix} 1 & 0 & 0 & 0 \\ 0 & 1 & 0 & 0 \\ 0 & 0 & 0 & 1 \\ 0 & 0 & 1 & 0 \end{pmatrix}, U_{\text{gate}} = \frac{1}{\sqrt{1+|s|^2}} \begin{pmatrix} 1 & 0 & s & 0 \\ 0 & s^* & 0 & 1 \\ s & 0 & 1 & 0 \\ 0 & 1 & 0 & s^* \end{pmatrix} \quad (10)$$

For $s = 0$ and $s = i$, U_{gate} can be written in terms of 2×2 Identity matrix (\mathcal{I}) and pauli matrices (σ_i 's) as,

$$\begin{aligned} U_{\text{gate}}(s = 0) &= \frac{1}{2} (\mathcal{I} \otimes \mathcal{I} + \mathcal{I} \otimes \sigma_z + \sigma_x \otimes \mathcal{I} - \sigma_x \otimes \sigma_z) \\ U_{\text{gate}}(s = i) &= \frac{1}{2} (e^{-\frac{i\pi}{4}} \mathcal{I} \otimes \mathcal{I} + e^{\frac{i\pi}{4}} \mathcal{I} \otimes \sigma_z + e^{\frac{i\pi}{4}} \sigma_x \otimes \mathcal{I} - e^{-\frac{i\pi}{4}} \sigma_x \otimes \sigma_z) \end{aligned}$$

Using Eq.(10) combination gate becomes

$$U_{\text{comp}} = U_{\text{gate}} U_{XOR} = \frac{1}{\sqrt{1+|s|^2}} \begin{pmatrix} 1 & 0 & 0 & s \\ 0 & s^* & 1 & 0 \\ s & 0 & 0 & 1 \\ 0 & 1 & s^* & 0 \end{pmatrix} \quad (11)$$

One applies U_{comp} gate to the initial state

$$U_{\text{comp}} |\Psi\rangle_i = \frac{1}{1+|z|^2} \frac{1}{\sqrt{1+|s|^2}} \begin{pmatrix} z^2 + s \\ z(s^* + 1) \\ sz^2 + 1 \\ z(s^* + 1) \end{pmatrix} \quad (12)$$

After this one applies post-selection operator (P),

$$P = \mathbf{I} \otimes |\uparrow\rangle_z \langle\uparrow| = \begin{pmatrix} 1 & 0 \\ 0 & 1 \end{pmatrix} \otimes \begin{pmatrix} 1 & 0 \\ 0 & 0 \end{pmatrix} = \begin{pmatrix} 1 & 0 & 0 & 0 \\ 0 & 0 & 0 & 0 \\ 0 & 0 & 1 & 0 \\ 0 & 0 & 0 & 0 \end{pmatrix} \quad (13)$$

Applying this post-selection operator on Eq.(12) one gets,

$$PU_{\text{comp}}|\Psi\rangle_i = P|\Psi(1)\rangle = \frac{1}{1+|z|^2} \frac{1}{\sqrt{1+|s|^2}} \begin{pmatrix} z^2 + s \\ sz^2 + 1 \end{pmatrix} \otimes |\uparrow\rangle_z \quad (14)$$

Ultimately by appropriate normalization (postselection) on the first qubit one gets the evolved first qubit state as,

$$|\tilde{\psi}\rangle = \frac{P|\Psi(1)\rangle}{\sqrt{\langle\Psi(1)|P|\Psi(1)\rangle}} = \frac{1}{\sqrt{1+|f(z)|^2}} \begin{pmatrix} f(z) \\ 1 \end{pmatrix}, \quad (15)$$

where $f(z) = \frac{z^2+s}{sz^2+1}$. This is the implementation of QCUs for generating first iterated state $|\tilde{\psi}\rangle$.

In the same way taking identical two qubit state $|\tilde{\psi}\rangle \otimes |\tilde{\psi}\rangle$ as initial state and following the steps from Eq.(9) to Eq.(15) one arrives at the second iterated state $|\tilde{\psi}\rangle_1$.

$$|\tilde{\psi}\rangle_1 = \frac{1}{\sqrt{1+|f^{(2)}(z)|^2}} \begin{pmatrix} f^{(2)}(z) \\ 1 \end{pmatrix}, \quad (16)$$

By repetition of the above process one eventually arrives at the n -th iterated desired state,

$$|\tilde{\psi}\rangle_{n-1} = \frac{1}{\sqrt{1+|f^{(n)}(z)|^2}} \begin{pmatrix} f^{(n)}(z) \\ 1 \end{pmatrix}, \quad (17)$$

It is worth pointing out that with successful generation (associated with success probability p_{success} of each successive desired iterated qubit state, the ensemble of identically prepared qubits reduces by a factor of 2 as iteration(n) increases. This is a manifestation of the fact that one really needs to start with $\left(\frac{2}{p_{\text{success}}}\right)^n$ no. of identically prepared qubits at the beginning to successfully generate the desired n -th iterated qubit state.

===== [5] Success Probability of the emulated dynamics induced by FNLC map for $s = i$

In this subsection of supplementary material, we provide the analytical form of success probability distribution for 1st iteration yielding the desired outcome of the emulated FNLC map (Eq.(2)) with $s = i$ and also present the average success probability of the first iteration to be successful (yielding the desired evolved state).

Following Eq.(13) we write the success probability (yielding the state in Eq.(14) in our favor as per our protocol) as,

$$p_{\text{success}} = \langle\Psi(1)|\hat{P}^\dagger\hat{P}|\Psi(1)\rangle = \frac{1+|z|^4}{(1+|z|^2)^2} \quad (18)$$

In fact we can replicate the same process for generating the desired n -th iterated state with the following success probability,

$$p_{\text{success}}(n) = \langle\Psi(1)|\hat{P}^\dagger\hat{P}|\Psi(1)\rangle = \frac{1+|f^{(n-1)}(z)|^4}{(1+|f^{(n-1)}(z)|^2)^2} \quad (19)$$

Given one can always write the initial state correspondent complex number z as $z = \cot \frac{\theta}{2} e^{i\phi}$ [39], the expression in Eq.(19) simplifies to,

$$p_{\text{success}}(n) = \frac{1}{4}(3 + \cos 2\theta_{n-1}) \quad (20)$$

which in turn gives the *average success probability* as,

$$\langle p_{\text{success}} \rangle = \frac{\int_{\theta} \int_{\phi} p_{\text{success}} \sin \theta d\theta d\phi}{\int_{\theta} \int_{\phi} \sin \theta d\theta d\phi} = \frac{2}{3} \quad (21)$$

===== [6] Roots of FNLC map for $s = i : f^{(2n+1)}(z) = 1$

We must point out that the statistical correlation of ensembles of K_3 data series is not very generic as shown in FIG.1. In fact the nature of this fantastic outcome of r_{XY} stabilizing towards zero is the manifestation of the fact that one of the eigenstates of the dichotomic operator is the fixed point of the map situated at $|+x\rangle$ (+ve eigenstate of σ_x) upon repeated discrete time evolution. Moreover, the randomness of correlation (as depicted in FIG.1) is solely because of the chaotic evolution of the initial states chosen from the Julia set.

Upon careful analysis we can say that experimentally it is only enough to measure the expectation value of the particular dichotomic measurement operator with the evolved initial states where eigenstates of the measurement operator satisfy $f^{(2n+1)}(z) = 1$. It turns out that there are several other measurement operator solutions ($\vec{\sigma} \cdot \hat{n}$) which are roots of this equation namely,

$$\hat{n} = -\hat{i}, \hat{j}, -\hat{j}, \frac{1}{\sqrt{2}}(\hat{i} + \hat{j}), \frac{1}{\sqrt{2}}(\hat{i} - \hat{j}), \frac{1}{\sqrt{2}}(-\hat{i} + \hat{j}), \frac{1}{\sqrt{2}}(-\hat{i} - \hat{j})$$

All these measurement operator will lead to the same qualitative outcome as FIG.1. It is also a good point to mention that in experiment we do not need to measure the evolution of the measurement operator eigenstates through QCU's once it reaches the fixed point situated at $|+x\rangle$. This reduces a significant number of QCU's used in the experiment.